

Spatial Dynamics of Chikungunya Virus, Venezuela, 2014

Appendix

1. Materials and Methods

1.1. Estimating the Reproductive Number (R_0)

For new emerging infectious diseases, the value of the reproductive number R_0 can be inferred indirectly from the initial epidemic phase by estimating the exponential epidemic growth rate (r) of new observed infections and relating these parameters to the generation time of infection (Tg) through the following equation (1).

$$R = \frac{1}{M(-r)}$$

where M is the moment generating function of the disease generation time distribution. A generation time distribution for chikungunya (CHIK) was defined using a gamma distribution with a mean of 1.86 weeks and a standard deviation of 0.05 weeks. This includes both the human and vector infection cycle, by assuming a short mosquito infection lifespan case as reported before by Boëlle et al. (2). For this method we applied the ‘ R_0 ’ package version 1.2–6 developed by Boëlle and Obadia (3) (The R-Development Core Team, <http://www.r-project.org>).

1.2. Estimating the Effective Reproductive Number (R_t)

Given that the behavior of the force of chikungunya virus (CHIKV) infection through time was unknown, we calculated a real-time estimate of the basic reproductive number of the disease, that is the effective reproductive number at time t (R_t) as originally proposed by Nishiura et al. (4). We then explored the time-varying transmissibility using the R_t series derived following the methodology of Coelho and Carvalho (5). Hence, R_t was estimated as

$$R_t = \left(\frac{Y_{t+1}}{Y_t} \right)^{1/n}$$

where Y_t and Y_{t+1} are taken to be the number of reported disease cases for a particular time t and $t+1$, respectively, while n defines the ratio between the length of the reporting interval and the mean generation time of the disease. The reporting interval was defined as the duration of an epidemiologic week (7 days), while the generation time was assumed to be of 2 weeks as established above. To run the calculation, we applied the R code developed by Coelho and Carvalho (5) available on the GitHub repository at <https://github.com/fccoelho/paperLM1> (The R-Development Core Team).

1.3. Trend Surface Analysis (TSA) and Local Vectors of Direction and Speed of Infection

TSA methodology consists in fitting, through the method of least squares, a function in a multiple-regression-like procedure where the response variable, in this case, *time*, is expressed as a polynomial function of geographic coordinates (X_i, Y_i) of individual case-points i. e., $time = f(X, Y)$, a model known as a polynomial regression (6). The order of the polynomial chosen as the best fit-model or the best polynomial equation will determine the shape of the curve or surface. Here, we used a third-order polynomial. The variable *time* (in days) was created using the symptoms onset date from the index case (IC) as the baseline date across the 810 case localities, this is, $time(X_i, Y_i)$. Thus, *time* is considered as the number of days elapsed between the appearance of a case in a specific locality Z_i and the IC. Results of the TSA were used to generate a contour map or smoothed surface, with each contour line representing a specific predicted time-period in this urban landscape setting since the initial invasion of the virus. Finally, we proceeded to estimate the local rate and direction of the spread of infection as the directional derivative at each case using the TSA fitted model to obtain local vectors that depicted the direction and speed (inverse of the slope along the direction of the movement) of infection propagation from each locality in X and Y directions. To this end, we calculated partial differential equations of *time* with respect to the X - and Y -coordinates, $(\partial TIME / \partial X$ and $\partial TIME / \partial Y)$ to obtain local vectors that depicted the direction and speed (inverse of the slope along the direction of the movement) of infection propagation from each locality in X and Y direction. The resultant vector for each case will represent, in turn, the overall velocity (in m/day) and direction of disease spread in each point. The set of vectors were assembled in a vector field and overlapped over the fitted surface to visualize the pattern of local spread of the virus along the urban landscape. TSA has been previously used to study pathogen dispersal processes in space and time (7). Further details of this methodology can be found in Moore (8)

and Adjemian et al. (9). All the analyses were carried out in R software (The R-Development Core Team). Maps of time contours and vectors were generated in the ArcGIS software (v.10.3, ESRI Corporation, Redlands, CA), while general maps were constructed using Quantum GIS 2.14.3 Essen (GNU—General Public License).

1.4. Kriging Interpolation

Kriging is a local interpolation method based on a set of linear regressions that determine the best combination of weights to interpolate the data points by minimizing the variance as derived from the spatial covariance in the data (10). The weights are based on the spatial parameters of a theoretical variogram model such that sampling locations within the spatial range (close distances) of influence has more weight on the predicted value than the distant locations. Although kriging and trend surface analysis share some features (i.e., to describe the general spatial trend), the local interpolation performed by kriging shows an enhanced picture of the local spatial pattern given that the kriged values are very close to the observed ones. Kriging analyses (and resulting surface maps) were carried out in the Geostatistics tool from the ArcGIS software (v.10.3, ESRI Corporation).

1.5. Spatiotemporal Analysis

Even though CHIKV was introduced into a naïve population, i.e., the individuals had a similar immunological likelihood of becoming infected, we wanted to assess the hypothesis of heterogeneity during disease transmission. In this sense we aimed to find whether aggregation of cases was present during the CHIK epidemic and if the likelihood of being infected could have varied depending on space and time distances. Thus, to identify general space-time aggregation (clusters) of CHIK transmission during the whole epidemic (28 weeks) we performed the Knox analysis (11) and the incremental Knox test (IKT) proposed by Aldstadt in 2007 (12) to identify linked transmission events.

1.5.1. Knox Test

This method measures potential space–time interactions by analyzing pairs of cases that belong to a particular space (distance) and time (days) window. This intuitive method provided simplicity and promptness (13). Yet, the Knox test requires prior selection of a “critical” time and distance to classify whether the pairs are close in space, or in time, or both. The test statistic, X , is the number of pairs of cases that are close in both space and time, and its calculated as

$$X(s, t) = \sum_{i=1}^N \sum_{j=1}^{i-1} a_{ij}^s a_{ij}^t$$

where s and t being the selected spatial and temporal distances, N is the number of cases, and the pair of cases are represented by i and j . The exact p value is obtained by the Monte Carlo procedure.

To select the “critical” value of space and time for our analysis, we performed a series of repetitions of the Knox method varying the time windows from 1 to 4 weeks (30 days in total) and the space window ranging from 25 to 200 m. Such analyses were made using the software ClusterSeer 2.0 (Terraseer, Ann Arbor, MI), which provides the graphical output of the space–time interactions (10.000 Monte Carlo iterations). The relative risk (RR) of each space and time window was calculated according to Tran et al. (14); where the RR is considered to be the ratio between the observed number of pairs of cases found at the space-distance s (in meters) and the time-distance t (in weeks) and the number of expected pairs of cases found at these same distances.

1.5.2. Incremental Knox Test

The incremental Knox test (IKT) is similar to other tests of the general hypothesis of space–time dependence (cases close to one another are much more likely to interact than cases far apart). However, this technique tests the interaction at specific time intervals rather than the more general space–time interaction hypothesis. The IKT examines consecutive links in the chain of transmission by identifying significant clusters in determined space and time intervals. The test assumes that cases that are nearer together than would be expected in the absence of an infectious process belong to one similar linked event of transmission (12).

Therefore, the IKT was used to understand in which time interval the clusters of cases of CHIK belonging to the same chain of transmission occurred helping to understand the linked transmission processes occurring in certain temporal span. The interval Knox statistic is formulated as

$$IK(s, t) = \sum_{i=1}^N \sum_{j=1}^{i-1} a_{ij}^s b_{ij}^t$$

Were s and t are the selected spatial and temporal distances, N is the number of cases, and the pair of cases are represented by i and j . When the cases i and j are time interval (t) apart $b_{ij}^t = 1$. The Monte Carlo procedure with 10.000 iterations was used to construct reference distribution for IK (Z values) and the test results are also reported as the epidemiologic notion of excess of risk (details of this methodology can be found in [12]). over the time intervals from 1 to 31 days, and space distances from 25 to 500 m (selected distances in metres: 25, 50, 75, 100, 125, 150, 175, 200, 300, 400, 500).

2. Results

From surveillance data collected during the months following the introduction of CHIKV, the dynamics and timing of the 810 chikungunya reported cases were studied. Appendix Figure 1 depicts the distribution of cases and cumulative cases along the 28 weeks of the chikungunya epidemic. Since the detection of the index case (IC) in June of 2014, the north-central region of Venezuela experienced a continuous reporting of chikungunya cases. During the first 9 weeks (epidemiologic week [EW] 21-EW 29), a low number of cases were reported. After EW 30 cases increased rapidly with the exponential growth of the epidemic being observed between EW 30 and EW 33. The cumulative cases during the EW 22–49 followed a logistic growth (Appendix Figure 1: $R = 0.99$, $n = 810$, $p < 0.05$) reaching the plateau at EW 44 (787 cases). The total growth rate estimated from the logistic fitted curve was 0.53 cases per EW.

2.1. Reproductive Number (R_0) and Effective Reproductive Number (R_t)

To better understand the CHIK transmission dynamic, the basic reproductive number (R_0) was calculated during the exponential growth of the epidemic, that is during (EW 21–EW 33). During these first 12 weeks, the maximum value of R_0 reached was equal to 3.7 secondary chikungunya cases per primary case. Furthermore, we estimated the effective reproductive number (R_t) with a reporting interval of 1 week, to assess changes of R_0 through time. The curve of R_t values fluctuates in time as shown in Appendix Figure 2, where the maximum value of R_t obtained was 4.7 (95% CI 2.4–7.1) occurring during the EW 31 (Appendix Figure 2). Both measures are similar in principle, and estimate the transmission dynamic of the disease whether is at the initial phase of the epidemic (R_0) or as an estimate for the whole epidemic (R_t). The usefulness of R_t is the possibility to estimate its uncertainty (confidence interval) throughout the epidemic curve. This could be relevant and applicable to other diseases as well. Due to the

intrinsic variability of the R_t series, the examination of its credible intervals is essential to identify periods of sustained transmission (5).

2.2. Kriging Interpolation

We performed an ordinary kriging using 3 anisotropic variogram models. The models were compared by cross-validation and evaluated in terms of their overall robustness: optimality and validity of the model to fit the observed data (Appendix Table 1, Appendix Figure 3). Overall, all the models underestimated the variability in their predictions as is shown by: i) negative values of the mean standardized errors (MSE), ii) average standard error (ASE) values lower than the root-mean-squared prediction error (RMSE) values, and iii) standardized root-mean-squared prediction error (RMSSE) values >1 (Appendix Table 1). This can be due to too few sampled locations within the spatial range of the study area. However, our best selected model (Gaussian) was the one that had the MSE nearest to 0, the smallest RMSE, the ASE nearest to the RMSE, and a RMSSE nearest to 1 (15).

The model was adjusted for the directional spatial trend of our data (anisotropy) in the semivariogram (10). Maps showing the kriging standard errors of the Gaussian model and of the other 2 models (for comparison) are presented in Appendix Figure 3. Darker colors in the error map (Appendix Figure 3) show larger kriging standard errors. Overall, the model failed to predict in areas out of the main spatial range of the data (where there are fewer and scarcer case locations) and showed a better prediction toward the south-west and eastern zones of the study area where a larger number of locations are presented. Indeed, this analysis identified a faster propagation of the epidemiologic wave at the south-west and eastern areas where the model showed its better fit (Appendix Figure 3, panel a), and a slower movement to the north-east and south-center areas.

2.3. Knox Test

The results obtained after the analysis with different critical values of s and t showed that the core clusters (main clusters) found at week 1 (25–200 m) are the same than those (core clusters) found at week 2, 3, and 4 (25–200 m), therefore, we have selected to show on Appendix Figure 4 the graphical output of the critical values of t with a fixed space window of 100 m. However, the size of the core clusters is susceptible to the change of the space and time

windows, making the clusters bigger or smaller in terms of number of links (Appendix Table 1), i.e., from 164 space-time links (1W,100 m) to 220 space-time links (3W,100 m).

Regarding the RR at different space and time windows (Appendix Table 1), the highest RR were found at the space–time window of 1 week and 25–200 m (RR = between 3 and 2), but also showing RR >1.5 up to week 3 at the same space windows, while from week 4, values showed RR <1.5 (Appendix Figure 5). These results provided useful information that allowed to observe the extent of the interaction of s and t values that shows the highest RR. Hence, RR values that show an important strength of association are present up to week 3 (21 days) within a distance that varies between 25 and 150 m. This agrees with previous results obtained by Vincenti-Gonzalez et al. (16) for Venezuela, where the significant hot spots of high dengue seroprevalence values were found between 25–100 m, suggesting a focal transmission.

Even though the RR in week 3 decreased along the different distances (average $32 \pm 7\%$) when compared to the RR of week 1, the RR remained higher than one (RR>1) in week 3. Given the fact that the Knox test results showed the same core clusters along the different t windows and the RR remained epidemiologically relevant after 3 weeks (general clustering of symptoms onset date, and RR>1), we used the window of 3 weeks with a distance window of 100 m to show the global clusters of transmission (Appendix Figure 6). We decided to choose these distance and time variables based on biologic and ecologic knowledge as explained in the manuscript and in agreement with other authors (17,18). Where 100 m is the distance referred by most as the average flight range radius of *Aedes* spp. and a time window of 3 weeks gives enough time span for most transmission events to occur (19–21).

2.3.1. General Clusters of Transmission Events During the Epidemic Wave of Chikungunya

Our results (Appendix Table 3) show that the average cluster duration since the symptoms onset of the first case to the symptoms onset of the last case within the clusters is 12.5 days ranging from 1–67 days. The choosing of 100 m does not preclude the finding of larger distances between cases within a cluster as the range of distances found was between 8–216 m. We expect that within clusters >1 chain of transmission will occur each with a duration of ~1 week or less.

2.4. Incremental Knox Test

The IKT was the second method used to assess the uncertainty of the cluster analysis. The previous was made employing an exploratory mode where the p-values (Appendix Figure 7) and the RR (Appendix Figure 8) were examined for a range of values of s and t . The results of the IKT analysis proved to be useful to identify linked transmission events, and showed that the temporal intervals with the strongest spatial clustering (belonging to the same chain of transmission) and RR occurs between 1–7 days suggesting multiple vector feeding within a gonotrophic cycle (22), with less strong clustering around 12–14 days. High RR results within 1 week are consistent for all tested distances, but values of $RR > 5$ were found to be in distances between 25 and 150 m (Appendix Figures 7, 8), favoring our previous selection of a space-time window of 100 m.

4. References

1. Wallinga J, Lipsitch M. How generation intervals shape the relationship between growth rates and reproductive numbers. *Proc Biol Sci.* 2007;274:599–604. [PubMed](#)
<http://dx.doi.org/10.1098/rspb.2006.3754>
2. Boëlle P-Y, Thomas G, Vergu E, Renault P, Valleron A-J, Flahault A. Investigating transmission in a two-wave epidemic of Chikungunya fever, Réunion Island. *Vector Borne Zoonotic Dis.* 2008;8:207–17. [PubMed](#) <http://dx.doi.org/10.1089/vbz.2006.0620>
3. Boëlle P-Y, Obadia T. ‘R0’: estimation of R0 and real-time reproduction number from epidemics. R package version 1.2-6. 2015. [2017 Dec 20]. <https://cran.r-project.org/web/packages/R0/R0.pdf>
4. Nishiura H, Chowell G, Heesterbeek H, Wallinga J. The ideal reporting interval for an epidemic to objectively interpret the epidemiological time course. *J R Soc Interface.* 2010;7:297–307. [PubMed](#) <http://dx.doi.org/10.1098/rsif.2009.0153>
5. Coelho FC, de Carvalho LM. Estimating the attack ratio of dengue epidemics under time-varying force of infection using aggregated notification data. *Sci Rep.* 2015;5:18455. [PubMed](#)
<http://dx.doi.org/10.1038/srep18455>
6. Legendre P, Legendre L. *Trend surface analysis. Numerical ecology.* Amsterdam: Elsevier Science; 1998. p. 739–46.

7. Pioz M, Guis H, Calavas D, Durand B, Abrial D, Ducrot C. Estimating front-wave velocity of infectious diseases: a simple, efficient method applied to bluetongue. *Vet Res (Faisalabad)*. 2011;42:60. [PubMed](#) <http://dx.doi.org/10.1186/1297-9716-42-60>
8. Moore DA. Spatial diffusion of raccoon rabies in Pennsylvania, USA. *Prev Vet Med*. 1999;40:19–32. [PubMed](#) [http://dx.doi.org/10.1016/S0167-5877\(99\)00005-7](http://dx.doi.org/10.1016/S0167-5877(99)00005-7)
9. Adjemian JZ, Foley P, Gage KL, Foley JE. Initiation and spread of traveling waves of plague, *Yersinia pestis*, in the western United States. *Am J Trop Med Hyg*. 2007;76:365–75. [PubMed](#) <http://dx.doi.org/10.4269/ajtmh.2007.76.365>
10. Dale M, Fortin M. *Spatial analysis: a guide for ecologists*. 2nd edition. Cambridge (UK): Cambridge University Press; 2014.
11. Knox EG. The detection of space-time interactions. *J R Stat Soc Ser C Appl Stat*. 1964;13:25–9.
12. Aldstadt J. An incremental Knox test for the determination of the serial interval between successive cases of an infectious disease. *Stochastic Environ Res Risk Assess*. 2007;21:487–500. <http://dx.doi.org/10.1007/s00477-007-0132-3>
13. Gear J. A test for detecting space-time clustering and a comparison with some existing methods [Doctoral dissertation]. Chapel Hill (NC): University of North Carolina; 2006:10–12. [2017 Dec 20]. <https://cdr.lib.unc.edu/indexablecontent/uuid:363bf6d4-373b-4d26-ae00-561e622d34af>
14. Tran A, Deparis X, Dussart P, Morvan J, Rabarison P, Remy F, et al. Dengue spatial and temporal patterns, French Guiana, 2001. *Emerg Infect Dis*. 2004;10:615–21. [PubMed](#) <http://dx.doi.org/10.3201/eid1004.030186>
15. Johnston K, Hoef M, Krivoruchko K, Lucas N. *Using ArcGIS geostatistical analyst*. Redlands, CA: ESRI; 2001.
16. Vincenti-Gonzalez MF, Grillet ME, Velasco-Salas ZI, Lizarazo EF, Amarista MA, Sierra GM, et al. Spatial analysis of dengue seroprevalence and modeling of transmission risk factors in a dengue hyperendemic city of Venezuela. *PLoS Negl Trop Dis*. 2017;11:e0005317. [PubMed](#) <http://dx.doi.org/10.1371/journal.pntd.0005317>
17. Vazquez-Prokopec GM, Kitron U, Montgomery B, Horne P, Ritchie SA. Quantifying the spatial dimension of dengue virus epidemic spread within a tropical urban environment. *PLoS Negl Trop Dis*. 2010;4:e920. [PubMed](#) <http://dx.doi.org/10.1371/journal.pntd.0000920>

18. Vazquez-Prokopec GM, Montgomery BL, Horne P, Clennon JA, Ritchie SA. Combining contact tracing with targeted indoor residual spraying significantly reduces dengue transmission. *Sci Adv.* 2017;3:e1602024. [PubMed http://dx.doi.org/10.1126/sciadv.1602024](http://dx.doi.org/10.1126/sciadv.1602024)
19. Harrington LC, Scott TW, Lerdthusnee K, Coleman RC, Costero A, Clark GG, et al. Dispersal of the dengue vector *Aedes aegypti* within and between rural communities. *Am J Trop Med Hyg.* 2005;72:209–20. [PubMed http://dx.doi.org/10.4269/ajtmh.2005.72.209](http://dx.doi.org/10.4269/ajtmh.2005.72.209)
20. Rudolph KE, Lessler J, Moloney RM, Kmush B, Cummings DA. Incubation periods of mosquito-borne viral infections: a systematic review. *Am J Trop Med Hyg.* 2014;90:882–91. [PubMed http://dx.doi.org/10.4269/ajtmh.13-0403](http://dx.doi.org/10.4269/ajtmh.13-0403)
21. Mbaika S, Lutomiah J, Chepkorir E, Mulwa F, Khayeka-Wandabwa C, Tigoi C, et al. Vector competence of *Aedes aegypti* in transmitting Chikungunya virus: effects and implications of extrinsic incubation temperature on dissemination and infection rates. *Viol J.* 2016;13:114. [PubMed http://dx.doi.org/10.1186/s12985-016-0566-7](http://dx.doi.org/10.1186/s12985-016-0566-7)
22. Aldstadt J, Yoon I-K, Tannitisupawong D, Jarman RG, Thomas SJ, Gibbons RV, et al. Space-time analysis of hospitalised dengue patients in rural Thailand reveals important temporal intervals in the pattern of dengue virus transmission. *Trop Med Int Health.* 2012;17:1076–85. [PubMed http://dx.doi.org/10.1111/j.1365-3156.2012.03040.x](http://dx.doi.org/10.1111/j.1365-3156.2012.03040.x)

Appendix Table 1. Model parameters of Kriging interpolation*

Model	Nugget (C_0)	Range (a)	Partial Sill (C_1)	MSE	RMSE	ASE	RMSSE
Gaussian	8.88						
	30.89			-0.014	17.35	14.29	1.18
	188.42						
Spherical	0.05						
	48.84			-0.015	17.45	11.04	1.53
	117.51						
Exponential	2.06						
	984.85			-0.016	18.13	15.07	1.40
	388.71						

*ASE, average standard error; MSE, mean standardized error; RMSE, root-mean-square error; RMSSE, root-mean-square standardized error.

Appendix Table 2. Knox test with alternative definitions of spatial and temporal proximity*

Time, wk	Distance, m	Expected	Observed	RR
1	25	22	72	3.27
	50	28	81	2.86
	75	45	117	2.57
	100	72	164	2.27
	125	97	213	2.20
	150	122	258	2.11
	175	159	316	1.99
	200	199	376	1.89
2	25	34	77	2.28
	50	44	95	2.18
	75	70	138	1.98
	100	110	202	1.83
	125	148	264	1.78
	150	187	322	1.72
	175	243	404	1.66
	200	304	497	1.63
3	25	43	79	1.85
	50	55	97	1.76
	75	88	144	1.63
	100	140	220	1.57
	125	188	293	1.56
	150	237	360	1.52
	175	308	457	1.48
	200	386	566	1.47
4	25	50	80	1.59
	50	65	99	1.53
	75	104	150	1.45
	100	164	236	1.44
	125	221	313	1.42
	150	279	383	1.37
	175	362	493	1.36
	200	453	617	1.36

*Monte Carlo simulations performed in each analysis:10.000.

Appendix Table 3. Description of the space–time cluster identified for the chikungunya epidemic in the north-central region of Venezuela*

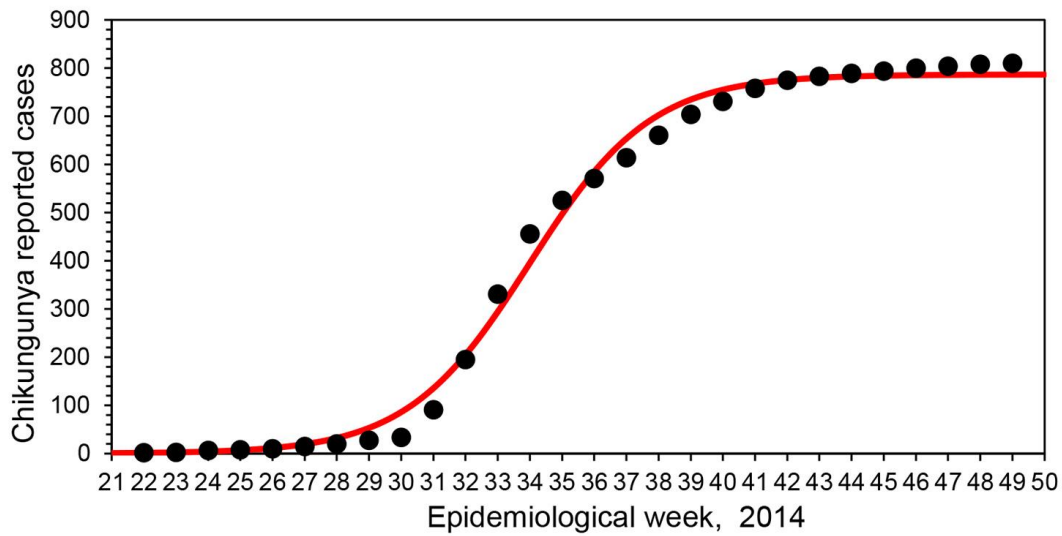
Cluster ID	No. cases	Day occurrence, first–last case	Cluster duration, d	Average distance from IC, m	Range of distance from IC, m	Velocity average, m/day	Velocity range, m/day
1	2	95–105	11	10132.0	10128–10136	102.0	97–107
2	4	77–105	29	7659.8	7636–7686	86.8	73–100
3	4	72–85	14	2556.0	2818–2613	32.3	30–36
4	3	72–94	23	2872.0	2857–2898	33.7	30–40
5	2	121–126	6	6685.5	6661–6710	54.0	53–55
7	3	0–25	26	31.7	0–95	1.3	0–4
8	2	125–135	11	2598.5	2598–2599	20.0	19–21
9	3	64–95	78	2553.7	2515–2585	33.3	27–34
10	5	71–99	29	2344.0	2299–2429	29.6	24–33
11	2	73–73	1	1857.0	1856–1858	25.0	25.0
12	2	61–61	1	3673.5	3673–3674	60.0	60.0
13	2	73–80	8	2550.0	2506–2594	33.4	32–34
14	4	79–107	29	2680.3	2647–2714	29.0	25–34
15	5	72–108	37	3463.0	3418–3508	43.4	32–51
16	3	43–57	15	3687.0	3680–3700	75.3	65–86
17	3	3–31	33	3015.3	3011–3020	45.3	39–50
18	2	91–99	9	3354.5	3315–3394	35.0	33–37
19	2	47–60	14	3305.0	3304–3306	62.5	55–70
20	3	63–78	16	3198.3	3192–3205	46.0	41–51
21	2	61–82	22	3531.5	3491–3571	50.5	44–57
23	2	66–66	1	3573.0	3571–3575	54.0	54.0
24	2	65–65	1	3684.0	3683–3685	57.0	57.0
25	9	59–72	14	3786.2	3734–3882	57.8	54–64
26	3	75–88	14	3967.0	3957–3967	53.0	45–53
27	12	69–77	9	4092.8	4008–4241	57.8	54–59
28	2	66–68	3	5608.5	5643–5574	83.5	83–84
29	3	0–66	67	6799.0	6194–6204	97.0	94–103
30	2	67–68	2	3617.0	3616–3618	53.5	53–54

Cluster ID	No. cases	Day occurrence, first–last case	Cluster duration, d	Average distance from IC, m	Range of distance from IC, m	Velocity average, m/day	Velocity range, m/day
31	2	74–80	7	3970.0	3929–3997	51.5	49–54
32	2	16–19	4	3822.0	3820–3824	220.0	201–239
33	5	65–82	18	4311.7	4282–4344	59.8	53–66
34	2	67–72	6	4483.0	4471–4495	64.5	62–67
35	2	88–94	7	5555.0	5554–5556	61.0	59–63
36	3	89–109	21	6709.7	6694–6739	67.7	61–76
37	2	72–76	5	4601.0	4571–4631	62.0	61–63
38	3	86–88	3	4760.3	4752–4775	54.3	54–55
39	3	68–86	19	4940.3	4894–4998	62.3	57–72
40	2	76–76	1	4645.5	4623–4668	61.0	61.0
41	2	61–64	4	4938.0	4938–4964	77.0	77–81
42	2	50–63	14	5138.0	5138.0	103.0	82–103
44	2	103–107	5	5561.5	5518–5605	53.0	52–54
45	2	116–117	2	5564.5	5562–5567	48.0	48.0
46	2	119–121	3	5596.0	5536–5556	47.0	47.0
47	2	108–115	8	5750.5	5727–5774	51.5	50–53
48	2	92–101	10	6126.5	6126–6127	64.0	61–67
49	2	80–80	1	6356.0	6349–6363	79.5	79–80
50	2	76–76	1	6368.5	6368–6369	84.0	84.0
51	3	103–132	30	6501.6	6512–6479	56.0	49–63
52	2	85–85	1	6796.5	6191–6202	73.0	73.0
53	2	75–111	37	6382.5	6373–6392	71.0	57–85
54	2	99–103	5	7305.5	7279–7332	72.5	71–74
55	2	92–103	12	7734.5	7704–7765	79.5	84–75
56	2	60–74	15	7046.0	7011–7081	106.5	96–117
57	6	60–77	18	7341.8	7262–7428	108.3	96–122
58	2	81–83	3	7526.5	7495–7558	92.0	91–93
59	3	63–72	10	7598.6	7535–7661	112.3	106–120
60	2	76–76	1	8228.5	8221–8626	108.0	86–97
61	2	72–76	5	8396.0	8381–8411	113.5	111–116
62	2	89–100	12	8647.5	8626–8669	91.5	86–97
63	2	86–86	1	8778.5	8774–8783	102.0	102.0
64	2	102–115	14	9355.0	9349–9361	86.5	81–92
65	2	76–76	1	8228.5	8221–8236	108.0	108.0
66	2	75–80	6	8406.0	8359–8453	108.5	106–111
67	2	80–80	1	8804.0	8783–8825	110.0	110.0
68	2	79–79	1	10419.5	10397–10442	132.0	132.0
69	2	83–84	2	10822.0	10819–10825	129.5	129–130
70	3	70–85	16	10653.7	10603–10679	135.7	125–153
71	2	142–163	22	11749.5	11726–11776	77.5	72–83
72	5	69–99	31	7611.0	7599–7622	103.4	77–110
73	2	59–81	23	7943.0	7920–7966	116.5	98–135
74	3	70–92	23	12291.7	12224–12341	153.7	134–175
75	2	134–136	3	9903.5	9903–9904	73.5	73–74
76	2	65–79	15	7636.5	7630–7643	107.5	97–118
77	2	78–78	1	1651.5	1644–1659	21.0	21.0
78	3	129–133	5	5477.0	5477.0	41.7	42.0

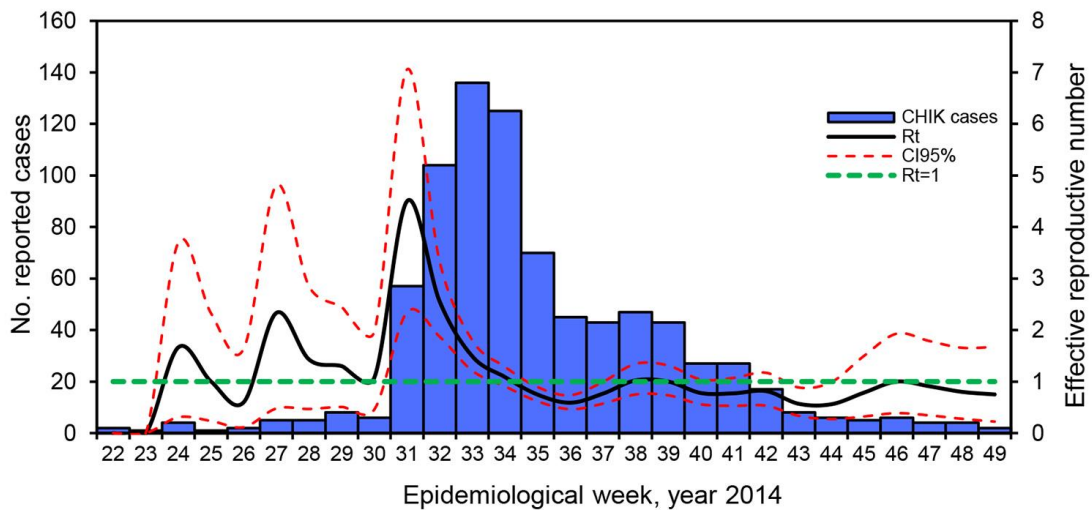
*Results shown here describes the general clusters of transmission found by Knox analysis with the critical values set at 100mts as clustering distance and 3 weeks as time window. Monte Carlo performed, 10,000.

Appendix Table 4. Linear distance between cases within the major spatiotemporal clusters

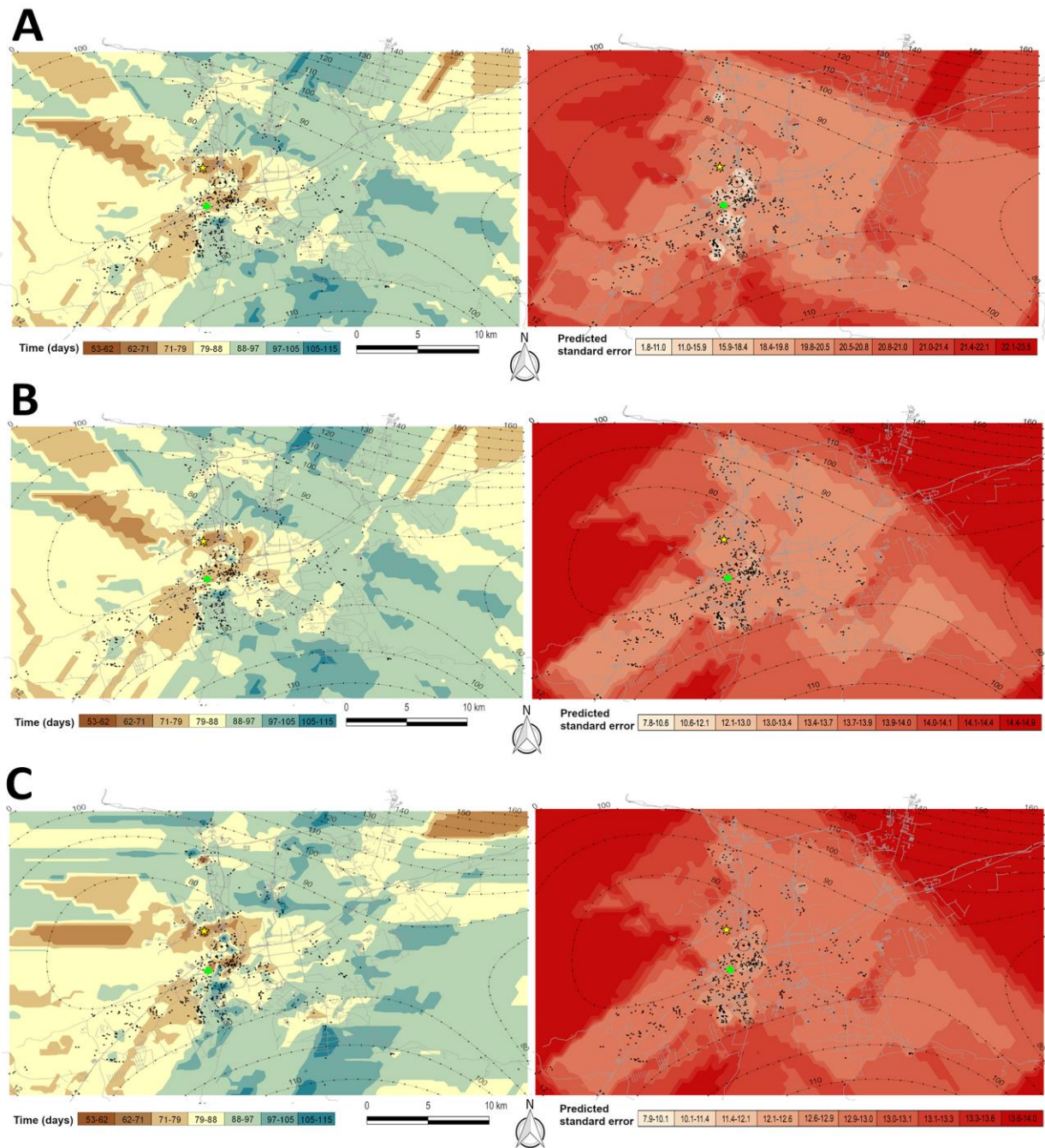
Cluster ID	No. cases	Average distance, m	Stddev, m	Maximum, m	Minimum, m
Cluster 10	5	77.0	47.2	130.7	16.2
Cluster 14	4	130.7	27.3	150.4	92.1
Cluster 15	5	63.6	23.7	85.4	30.0
Cluster 02	4	38.2	16.4	54.6	21.9
Cluster 25	9	61.9	26.5	66.4	26.2
Cluster 27	12	81.6	19.2	216.0	8.0
Cluster 33	5	78.6	1.1	79.8	77.6
Cluster 33	4	85.6	26.5	105.0	55.4
Cluster 57	6	77.8	28.9	124.0	54.1
Cluster 72	5	56.7	39.1	93.7	10.3
Average	6	75.2	25.6	110.6	39.2



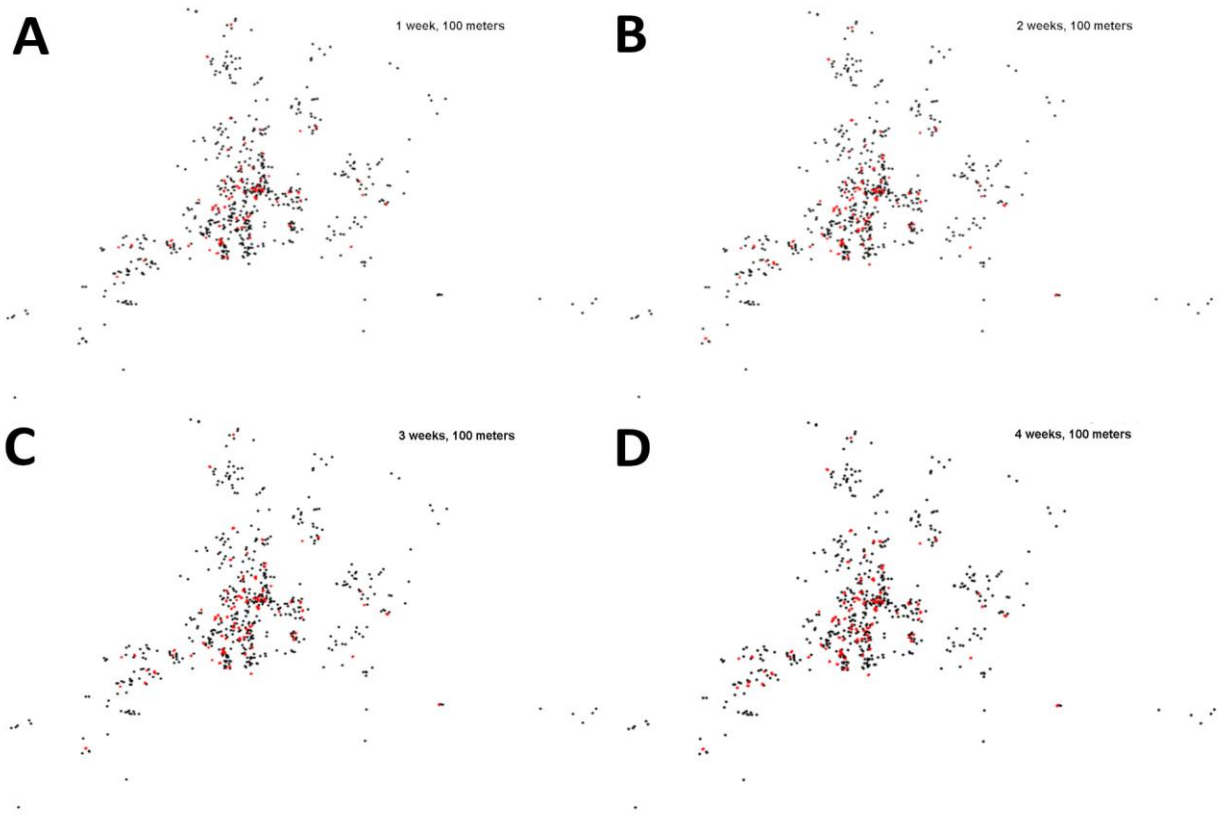
Appendix Figure 1. Logistic fitted model for reported chikungunya cases during the epidemic of 2014 in Carabobo State, Venezuela. Chikungunya cases are depicted by open black dots, red line depicts the fitted curve (logistic model).



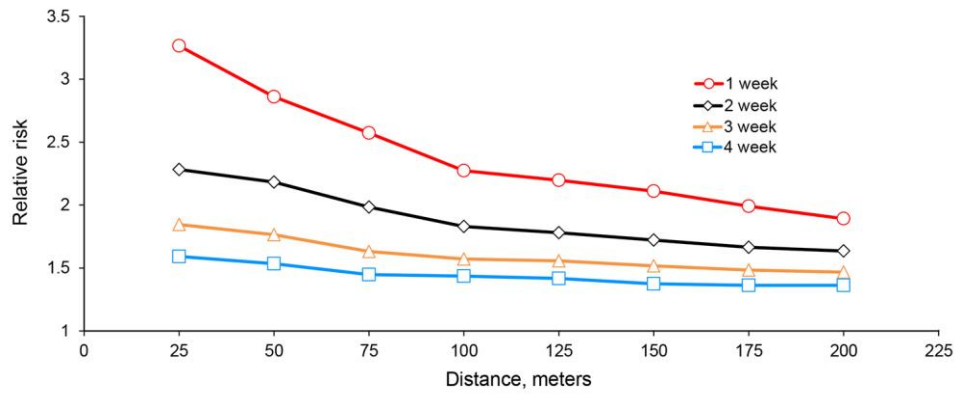
Appendix Figure 2. Reproduction number of chikungunya fever in Carabobo State, Venezuela, during 2014. Blue bars show the epidemic curve; the cases are shown in a weekly interval. Solid black line corresponds to the estimated R_t for the epidemic, dashed red line depicts the 95% CI, whereas green dashed line depicts the threshold $R_t = 1$.



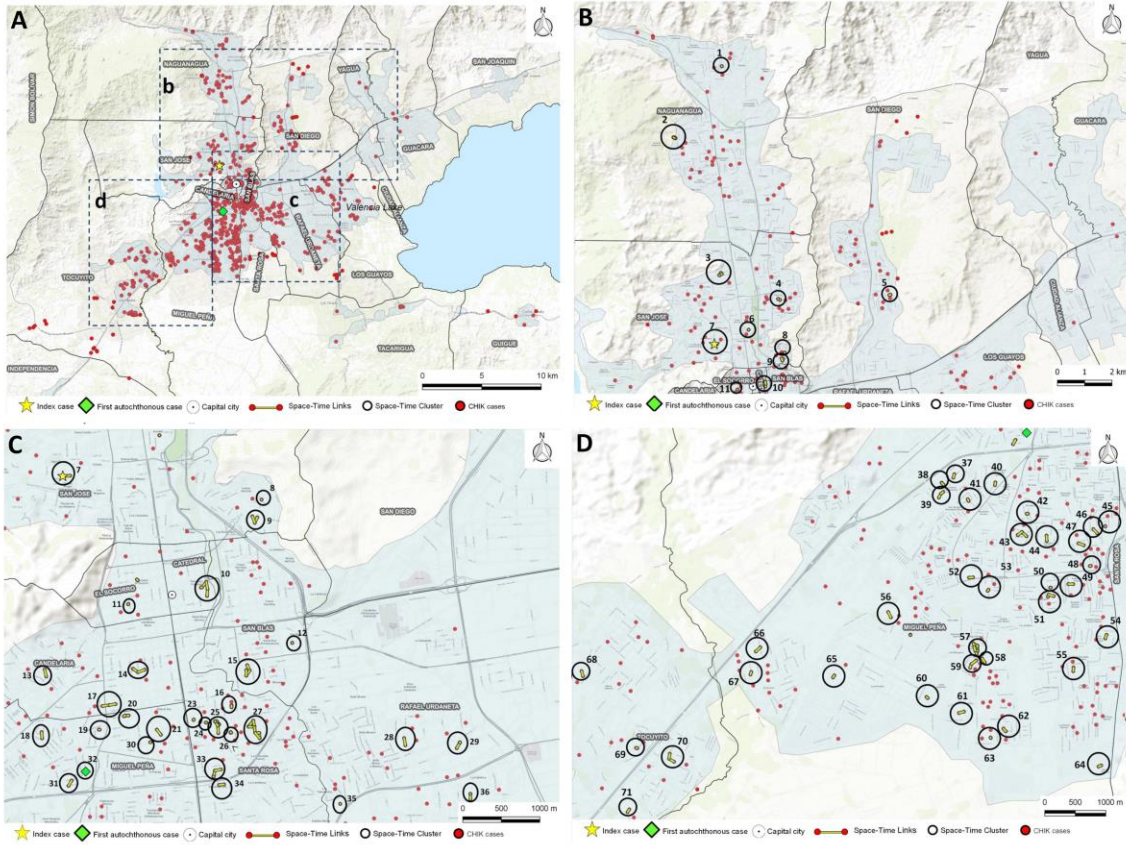
Appendix Figure 3. Spatial prediction map for the ordinary kriging interpolation of number of days elapsed between the appearance of a case in a specific locality and the IC obtained using the Gaussian (A), spherical (B), and exponential (C) models. Surface maps showing the kriging standard errors for each model in the right side of each map.



Appendix Figure 4. Space–time output varying the time window from 1 to 4 weeks. In red, the space-time clusters. Distance window was set at 100 m.



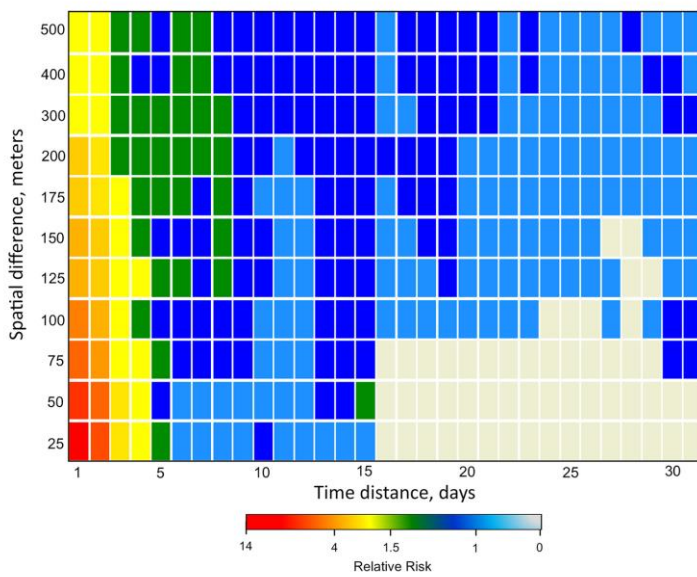
Appendix Figure 5. Relative risk from the Knox test with alternative definitions of spatial and temporal proximity.



Appendix Figure 6. A) Geographic distribution of chikungunya reported cases in Carabobo state, Venezuela. a) Red dots denote case location, black dashed lines (b, c, d) are the different panels division (arbitrary) within Carabobo state selected to show in detail (zoom in) the general clusters of transmission. B) Geographic distribution and significant space–time clustering of chikungunya reported cases. Zoom in of the different cluster of transmission detected (including the IC), red dots denote case location, black circles identify a significant space–time cluster and yellow lines shows the interaction between cases (time–space link). The analysis was performed using 100 m as clustering distance and 3 weeks as time window. Significance level for local clustering detection was of 0.05. C) Geographical distribution and significant space-time clustering of chikungunya reported cases. Zoom in of the different cluster of transmission detected (including IC and AC), red dots denote case location, black circles identify a significant space-time cluster and yellow lines shows the interaction between cases (time-space link). The analysis was performed using 100 m as clustering distance and 3 weeks as time window. Significance level for local clustering detection was of 0.05. D) Geographic distribution and significant space–time clustering of chikungunya reported cases. Zoom in of the different cluster of transmission detected (including IC and AC), red dots denote case location, black circles identify a significant space–time cluster and yellow lines shows the interaction between cases (time–space link). The analysis was performed using 100 m as clustering distance and 3 weeks as time window. Significance level for local clustering detection was of 0.05.

		Distance, meters										
		25	50	75	100	125	150	175	200	300	400	500
Time, d.	1	0.00	0.00	0.00	0.00	0.00	0.00	0.00	0.00	0.00	0.00	0.00
	2	0.00	0.00	0.00	0.00	0.00	0.00	0.00	0.00	0.00	0.00	0.00
	3	0.00	0.00	0.00	0.00	0.00	0.00	0.00	0.00	0.00	0.00	0.00
	4	0.00	0.00	0.00	0.00	0.00	0.00	0.00	0.00	0.00	0.00	0.00
	5	0.12	0.13	0.00	0.02	0.01	0.02	0.00	0.00	0.00	0.00	0.00
	6	0.76	0.83	0.07	0.02	0.00	0.00	0.00	0.00	0.00	0.00	0.00
	7	0.87	0.90	0.22	0.04	0.03	0.02	0.00	0.00	0.00	0.00	0.00
	8	0.59	0.81	0.15	0.03	0.00	0.00	0.00	0.00	0.00	0.00	0.00
	9	0.86	0.95	0.48	0.52	0.10	0.02	0.12	0.08	0.04	0.05	0.01
	10	0.53	0.76	0.67	0.86	0.23	0.19	0.54	0.46	0.11	0.04	0.01
	11	0.81	0.73	0.62	0.76	0.68	0.63	0.88	0.64	0.37	0.06	0.03
	12	0.91	0.83	0.80	0.86	0.88	0.82	0.74	0.28	0.03	0.00	0.00
	13	0.79	0.26	0.15	0.24	0.16	0.20	0.08	0.02	0.04	0.00	0.00
	14	0.76	0.22	0.50	0.34	0.27	0.36	0.12	0.01	0.04	0.00	0.01
	15	0.74	0.11	0.22	0.14	0.11	0.22	0.26	0.20	0.33	0.04	0.10
	16	1.00	0.95	0.99	0.92	0.89	0.89	0.75	0.42	0.64	0.59	0.60
	17	1.00	0.99	0.99	0.97	0.67	0.59	0.49	0.40	0.63	0.40	0.43
	18	1.00	0.98	0.98	0.95	0.60	0.29	0.13	0.03	0.17	0.06	0.02
	19	1.00	0.98	0.98	0.83	0.53	0.44	0.38	0.32	0.15	0.01	0.00
	20	1.00	1.00	0.99	0.98	0.96	0.78	0.68	0.64	0.22	0.03	0.01
	21	1.00	1.00	1.00	0.91	0.96	0.94	0.93	0.94	0.43	0.08	0.11
	22	1.00	1.00	0.99	0.94	0.92	0.87	0.69	0.74	0.67	0.77	0.61
	23	0.98	0.99	0.98	0.87	0.90	0.96	0.82	0.78	0.65	0.24	0.26
	24	0.97	0.99	1.00	1.00	0.98	0.99	0.88	0.94	0.79	0.76	0.78
	25	0.97	0.99	1.00	0.99	0.97	0.98	0.94	0.98	0.81	0.65	0.74
	26	1.00	1.00	1.00	0.99	0.96	0.98	0.95	0.98	0.92	0.97	0.87
	27	1.00	1.00	1.00	0.96	0.98	0.99	0.98	1.00	1.00	0.96	0.82
	28	0.96	0.99	0.99	0.98	0.99	1.00	0.99	0.96	0.92	0.61	0.43
	29	0.96	0.98	0.96	0.90	0.99	0.99	1.00	0.95	0.54	0.30	0.61
	30	0.96	0.92	0.35	0.36	0.65	0.61	0.83	0.52	0.10	0.28	0.65
	31	1.00	0.98	0.32	0.33	0.62	0.66	0.86	0.86	0.38	0.80	0.91

Appendix Figure 7. Significant values of the exploratory IKT analysis. In red the significant (p value <0.05) of space–time interactions within the specific space–time intervals.



Appendix Figure 8. Values of relative risk for the exploratory IKT analysis. The colors in the heatmap depict the range of values of RR (refer to the legend) within the specific space–time intervals.